J. Fluid Mech. (1985), *vol.* 150, *pp.* 395–416
Printed in Great Britain

A numerical study of water-wave modulation based on a higher-order nonlinear Schrödinger equation

By EDMOND LO AND CHIANG C. MEI
Department of Civil Engineering, Massachusetts Institute of Technology

(Received 10 March 1983 and in revised form 31 July 1984)

In existing experiments it is known that the slow evolution of nonlinear deep-water waves exhibits certain asymmetric features. For example, an initially symmetric wave packet of sufficiently large wave slope will first lean forward and then split into new groups in an asymmetrical manner, and, in a long wavetrain, unstable sideband disturbances can grow unequally to cause an apparent downshift of carrier-wave frequency. These features lie beyond the realm of applicability of the celebrated cubic Schrödinger equation (CSE), but can be, and to some extent have been, predicted by weakly nonlinear theories that are not limited to slowly modulated waves (i.e. waves with a narrow spectral band). Alternatively, one may employ the fourth-order equations of Dysthe (1979), which are limited to narrow-banded waves but can nevertheless be solved more easily by a pseudospectral numerical method. Here we report the numerical simulation of three cases with a view to comparing with certain recent experiments and to complement the numerical results obtained by others from the more general equations.

1. Introduction

Since the discovery by Benjamin & Feir (1967) of the instability of weakly nonlinear Stokes waves by sideband disturbances, rapid advances have taken place in both theory and experiment on the behaviour of deep-water waves. In particular, the nonlinear evolution subsequent to the initial instability has been studied by using either a pair of conservation equations (Chu & Mei 1970) or, equivalently but more conveniently, the cubic Schrödinger equation (CSE) (Zakharov & Shabat 1972; Lake *et al.* 1977; Yuen & Ferguson 1978). These equations govern the slow modulation of the wave envelope, with a third-order accuracy in the wave slope ka. Among the theoretical predictions on the nonlinear evolution, recurrence is the most prominent feature.

Several existing experiments (Feir 1967; Lake *et al.* 1977; Melville 1982) were performed in relatively short tanks. In order to accelerate the nonlinear development the wave slopes were typically rather high. Detailed comparisons show that the observations agree with the third-order slow-modulation theory only in the early stages. Specifically, Feir (1967) examined the evolution of wave packets whose envelopes were initially symmetrical and bell-shaped. For larger values of maximum ka the envelopes became forward-leaning after a short distance from the wavemaker (4 feet); further downstream (28 feet) two prominent groups emerged, with the smaller group trailing. On the other hand the CSE, which is symmetric with respect to the spatial coordinate in the coordinate system moving at the group velocity, only predicts symmetric envelopes if they are symmetrical initially (Chu & Mei 1971; Yuen & Ferguson 1978). More comprehensive experiments for wave packets of various

durations in a much longer wave tank (130 m) have now been reported by Su (1982) and by Chereskin (1982). For short pulses their results extend those of Feir and reveal further information on group splitting and frequency downshift in the leading group. In the instability experiments of a uniform wavetrain (Lake *et al.* 1977; Melville 1982), the typical value of ka is greater than 0.2. The sideband disturbances, if they were of equal magnitude initially, were found to grow at equal rate only for a limited time. As nonlinearity became more and more important, the lower sideband grew faster and attained a greater maximum than the upper sideband, while the carrier wave dropped to a minimum. Before reaching these extrema, local breaking was observed in Melville's records and probably also occurred in those of Lake *et al.* This unequal growth has been suggested by Lake *et al.* as a possible contributor to the downward shift of the spectral peak of wind waves with increasing fetch. Again, the unequal growth of sidebands is not predicted by the CSE (Yuen & Ferguson 1978). From the experimental data, it can be inferred that significant departure from the numerical predictions by CSE occurs when the dimensionless time of evolution $(ka)^2\omega t$ has exceeded about 10, which is beyond the realm of applicability of the CSE.

Aside from the CSE, which is limited to slowly modulated waves, i.e. waves with a narrow spectral band, numerical studies of nonlinear evolution have been carried out previously via mode-coupling equations by West, Watson & Thomson (1974), Cohen, Watson & West (1976) and Bryant (1982). In their approaches the field equations are approximated to third order in wave slope ka and decomposed into a large number of propagating Fourier modes. The modal amplitudes are governed by simultaneous, cubically coupled ordinary differential equations. These equations are solved numerically by keeping a finite number of modes. Their results already exhibit trends toward asymmetry in the nonlinear stage. Another approach under similarly generous assumptions is the Zakharov equation, which has been used to deduce analytically criteria on linear instability (Crawford *et al.* 1981). These criteria are strikingly close to the accurate numerical solution of Longuet-Higgins (1978) for arbitrary ka. For nonlinear evolution the Zakharov equation must be discretized, leading also to mode-coupling equations which resemble those of West *et al.* (1974). Using only 7 Fourier modes, Yuen & Lake (1982) have shown further interesting features, including restabilization at very large ka.

While these general equations are more versatile, they are comparatively expensive for accurate numerical computations. If one is primarily interested in narrow-banded waves, an alternative is to extend the CSE by adding higher-order terms in order to enlarge its range of validity. The first attempt in this direction was made by Roskes (1977), who found numerically that an initially symmetric soliton envelope split into two soliton-like envelopes asymmetrically, in qualitative agreement with the observations of Feir (1967). However, his envelope equation did not include all the fourth-order terms. Correct fourth-order terms were later derived by Dysthe (1979) as cited in (2.1)–(2.4) in §2 below. The resulting equations enlarge the time range of validity from $(ka)^2\omega t = O(1)$ to $(ka)^3\omega t = O(1)$. He uses them to study analytically the initial instability of infinitesimal sideband disturbances, and finds that for the linear analysis all the higher-order terms except the last in (2.1) can be omitted. Janssen (1983) uses the simplified Dysthe equations to explain the unequal sideband growth in the nonlinear stage. As will be pointed out later, the most important contributions to the asymmetric development at large time are unfortunately associated with the discarded terms.

In this paper we shall apply a pseudospectral method which can solve efficiently Dysthe's equations in their full form and examine three examples. In the first of these,

the initial wave spectrum consists of two lines of equal height; thus there are two first-order sidebands but no carrier wave. Detailed comparison with some recent experiments by Keller (1982) will be made. In the second example of wave-packet evolution, comparison with recent experiments by Su (1982) will also be made. Finally, for a uniform wavetrain subjected to periodic sideband disturbances, we present some results showing the effect of dissipation on the long-time evolution.

In the coastal seas the change in water depth must be one of the factors affecting the long-distance propagation of waves. For sufficiently gradual depth variation Dysthe's approximation can be quite easily modified and solved numerically. Such computations are of value in interpreting sea-surface records by remote sensing, and will be reported in the future.

2. The governing equations

We first cite Dysthe's equations, which are valid for water so deep that $kh = O(ka)^{-1} \gg 1$.† In physical variables, let A be the complex amplitude of the first harmonic of the Stokes waves, A^* the complex conjugate of A, and ϕ the potential of the induced mean current. With minor corrections, the equations governing the slow variation of A and ϕ are (Dysthe 1979)

$$\frac{\partial A}{\partial t}+\frac{\omega}{2k}\frac{\partial A}{\partial x}+\mathrm{i}\frac{\omega}{8k^2}\frac{\partial^2 A}{\partial x^2}+\frac{\mathrm{i}}{2}\omega k^2|A|^2A-\frac{1}{16}\frac{\omega}{k^3}\frac{\partial^3 A}{\partial x^3}-\frac{\omega k}{4}A^2\frac{\partial A^*}{\partial x}$$
$$+\tfrac{3}{2}\omega k|A|^2\frac{\partial A}{\partial x}+\mathrm{i}kA\frac{\partial \phi}{\partial x}\Big|_{z=0}=0, \quad (2.1)$$

$$\frac{\partial^2\phi}{\partial x^2}+\frac{\partial^2\phi}{\partial z^2}=0 \quad (-h<z<0), \quad (2.2)$$

$$\frac{\partial\phi}{\partial z}=\frac{\omega}{2}\frac{\partial|A|^2}{\partial x} \quad (z=0), \quad (2.3)$$

$$\frac{\partial\phi}{\partial z}=0 \quad (z=-h). \quad (2.4)$$

The first four terms in (2.1) comprise the cubic Schrödinger equation in the fixed frame of reference. The linear x-derivatives of A represent the effects of frequency dispersion. These equations were derived under the assumption that $O(kA)=O(\partial A/\partial x)=O(ka)\ll 1$. Thus the additional terms due to Dysthe are $O(ka)^4$. The velocity of the induced current is $O(ka)^3$. We remark that Dysthe's equations can be derived from Zakharov's integral equation (Stiassnie 1984) by adding the narrow-band assumption.

It is advantageous to change to a coordinate system moving at the linear group velocity. We introduce following dimensionless variables:

$$\left.\begin{aligned} &A=a_0A', \quad \phi=\omega a_0^2\phi', \\ &\epsilon\omega\gamma\left(\frac{2k}{\omega}x-t\right)=\xi, \quad \epsilon k\gamma z=z', \\ &\epsilon^2kx=\eta, \quad \epsilon\gamma kh=h', \end{aligned}\right\} \quad (2.5)$$

where $\epsilon=ka_0$ and γ is a scale factor which renders the computational domain in ξ to 2π. To a fixed observer ξ is the negative of time elapsed and η is the distance over

† Dysthe assumes $kh>O(ka)^{-1}$. Since (2.2) implies that the horizontal and vertical lengthscales for ϕ are both $O(ka)^{-1}$, we can allow $kh=O(ka)^{-1}$ and (2.4).

which the group has advanced, i.e. the *fetch*. In this coordinate system the linear term A_{xx} in (2.1) generates an additional fourth-order term $\epsilon A_{\epsilon\eta}$, which is eliminated by making use of the leading-order part (the CSE) for A_η. With the primes omitted for brevity, the normalized equations become

$$\frac{\partial A}{\partial \eta}+\mathrm{i}\gamma^2\frac{\partial^2 A}{\partial \xi^2}+\mathrm{i}\,|A|^2A+8\epsilon\gamma\,|A|^2\frac{\partial A}{\partial \xi}+4\mathrm{i}\epsilon\gamma A\frac{\partial \phi}{\partial \xi}\bigg|_{z=0}=0, \tag{2.6}$$

$$4\frac{\partial^2\phi}{\partial \xi^2}+\frac{\partial^2\phi}{\partial z^2}=0 \quad (-h<z<0), \tag{2.7}$$

$$\frac{\partial \phi}{\partial z}=\frac{\partial}{\partial \xi}|A|^2 \quad (z=0), \tag{2.8}$$

$$\frac{\partial \phi}{\partial z}=0 \quad (z=-h). \tag{2.9}$$

We remark that the usual coordinate transformation is to use ξ and $\tau=\epsilon^2\omega\gamma t$. While the difference is immaterial for the CSE, it simplifies the fourth-order terms in (2.6). In particular, there is no longer a triple derivative, which can cause a minor numerical noise at a certain higher harmonic in the pseudo-spectral method to be described, since the terms A_{xxx} and A_{xx} in (2.1) cancel for that harmonic.

We shall always perform our computations in a periodic domain of period 2π. Thus the boundary conditions are

$$A(0,\eta)=A(2\pi,\eta), \tag{2.10}$$

$$\phi(0,z,\eta)=\phi(2\pi,z,\eta). \tag{2.11}$$

The initial value of $A(\xi,0)$ will be specified later for $\xi\in[0,2\pi]$.

For direct comparison with experiments we shall need the free-surface displacement $\zeta(\xi,\eta)$, which can be evaluated from A. In the dimensionless variables of (2.5) with $\zeta=a\zeta'$, the surface displacement is (after omitting primes)

$$\zeta(\xi,\eta)=\epsilon^2\gamma\frac{\partial \phi}{\partial \xi}\bigg|_{z=0}+\left\{\left(\tfrac{1}{2}A-\frac{\mathrm{i}\epsilon\gamma}{2}\frac{\partial A}{\partial \xi}-\frac{3\epsilon^2}{16}|A|^2A\right)\mathrm{e}^{\mathrm{i}\psi}\right.$$
$$\left.+\left(\frac{\epsilon}{4}A^2-\mathrm{i}\epsilon^2\gamma A\frac{\partial A}{\partial \xi}\right)\mathrm{e}^{2\mathrm{i}\psi}+\left(\frac{3\epsilon^2}{16}A^3\right)\mathrm{e}^{3\mathrm{i}\psi}\right\}+\{*\}, \tag{2.12}$$

where $\psi=-\eta/\epsilon^2+\xi/\epsilon\gamma$ is the phase function of the carrier waves. To compare this displacement with measurements at stationary probes, we must return first to the fixed coordinate system defined in (2.5). Note that, as ξ varies from 0 to 2π, the dimensional time t at a fixed dimensional distance $x_0=\eta/\epsilon^2k$ from the wavemaker varies from $2kx_0/\omega$ to $2kx_0/\omega-2\pi/\gamma\epsilon\omega$. Since the spectrum of the measured free-surface displacement can be approximately separated for each harmonic, for ready comparison with experiments we shall present the total first harmonic A' accurate to third order,

$$A'=A-\mathrm{i}\epsilon\gamma\frac{\partial A}{\partial \xi}-\frac{3\epsilon^2}{8}|A|^2A, \tag{2.13}$$

instead of A except when the difference between them is qualitatively noteworthy. The frequency deviation $\Delta\omega$ from ω is then proportional to the time derivative of the phase of A'. In terms of the dimensionless variables of (2.5),

$$\frac{\Delta\omega}{\omega}=\epsilon\gamma\frac{\partial\theta}{\partial\xi}, \tag{2.14}$$

where θ is the phase of A'.

We remark that the cubic Schrödinger equation for A is even in ξ; hence if $A(\xi,0)$ is symmetric in ξ so is $A(\xi,\eta)$ for all η. But A' or ζ contain odd derivatives of A and hence can be asymmetric. This type of asymmetry is, however, of higher order and cannot account for that observed in the experiments. Furthermore, it emphasizes the upper sideband more than the lower sideband. Now the 5th, 6th and 7th terms in (2.1) or the 4th term in (2.6) are odd derivatives in x; hence they contribute to the asymmetry in A directly. Since their effects become of first order after a time $(ka)^3\omega t = O(1)$ this asymmetry is very important. On the other hand, the last (current) term in (2.1) or (2.6) is an even derivative because of (2.3) and does not cause asymmetry in A directly. In Janssen's nonlinear theory only the last of the higher-order terms in (2.1) is kept; it cannot give a complete result, as will be discussed further in §6.

3. The numerical scheme

At any spatial step η, we first use the known value of $A(\xi,\eta)$ for all $0<\xi<2\pi$ from earlier computations to solve for the current potential ϕ by the pseudo-spectral method, as described in Fornberg & Whitham (1978). The spatial period is discretized by $2N$ points at which $A(\xi,\eta)$ is known. Transforming to the discretized Fourier space, we have

$$\hat{A}(\nu,\eta) = \mathrm{F}\{A(\xi,\eta)\} = \sum_{n=0}^{2N-1} A(n\,\Delta\xi,\eta)\,\mathrm{e}^{\mathrm{i}n\nu\pi/N},$$
$$\nu = 0, \pm1, \pm2, \ldots, \pm N, \ \Delta\xi = \pi/N. \quad (3.1)$$

Thus the number of Fourier modes is $2N+1$. The inverse transformation is

$$A(n\,\Delta\xi,\eta) = \mathrm{F}^{-1}\{\hat{A}(\nu,\eta)\} = \frac{1}{2N}\sum_{\nu=-N}^{\nu=N} \mu_\nu \hat{A}(\nu,\eta)\,\mathrm{e}^{-\mathrm{i}n\nu\pi/N}, \quad (3.2)$$

where $\mu_\nu = 1$ for $\nu \neq \pm N$ and $\frac{1}{2}$ for $\nu = \pm N$. Fourier modes with $\nu >$ or < 0 will be called the lower or upper sidebands. These transforms are readily evaluated by standard routines of fast Fourier transform (FFT). The derivatives of A with respect to ξ are given by

$$\frac{\partial^s A}{\partial \xi^s} = \mathrm{i}^s \mathrm{F}^{-1}\{(-\nu)^s\,\hat{A}(\nu,\eta)\} = \mathrm{i}^s\,\mathrm{F}^{-1}\{(-\nu)^s\,\mathrm{F}\{A(\xi,\eta)\}\}. \quad (3.3)$$

With the current potential similarly transformed,

$$\hat{\phi}(\nu,z,\eta) = \sum_{n=0}^{2N-1} \phi(n\,\Delta\xi,z,\eta)\,\mathrm{e}^{\mathrm{i}n\nu\pi/N}, \quad (3.4a)$$

$$\phi(n\,\Delta\xi,z,\eta) = \frac{1}{2N}\sum_{\nu=-N}^{\nu=N} \mu_\nu \hat{\phi}(\nu,z,\eta)\,\mathrm{e}^{-\mathrm{i}n\nu\pi/N}, \quad (3.4b)$$

(2.7), (2.8) and (2.9) become

$$\frac{\partial^2\hat{\phi}}{\partial z^2} - 4\nu^2\hat{\phi} = 0 \quad (h<z<0), \quad (3.5a)$$

$$\frac{\partial\hat{\phi}}{\partial z} = 2\mathrm{F}\{\mathrm{Re}\,(A^*\mathrm{i}\mathrm{F}^{-1}\{-\nu\,\mathrm{F}\{A\}\})\} \quad (z=0), \quad (3.5b)$$

$$\frac{\partial\hat{\phi}}{\partial z} = 0 \quad (z=-h). \quad (3.5c)$$

The solution can be readily written as

$$\hat{\phi}(\nu, z, \eta) = \mathrm{F}\{\mathrm{Re}\,(A^* \mathrm{iF}^{-1}\{-\nu\,\mathrm{F}\{A\}\})\}\frac{\cosh(2\nu(z+h))}{\nu\sinh(2\nu h)}, \tag{3.6}$$

and for use in (2.6),

$$\left.\frac{\partial\phi}{\partial\xi}\right|_{z=0} = \mathrm{iF}^{-1}\{-\nu\hat{\phi}\}_{z=0} = \mathrm{F}^{-1}\{-\mathrm{iF}\{\mathrm{Im}\,(A^*\mathrm{F}^{-1}\{-\nu\mathrm{F}\{A\}\})\}\coth(2\nu h)\}. \tag{3.7}$$

Note that we have discarded in $\partial\phi/\partial\xi$ an integration constant (function of η) that affects the phase of A only. In all our computations we consider only infinitely deep water; thus we have let

$$\coth 2\nu h = \pm 1 \quad \text{for } \nu \gtrless 0. \tag{3.8}$$

Having found $\phi_\xi(\xi, z, \eta)$, (2.6) is solved for $A(\epsilon, \eta)$ by a split-step Fourier method (Tappert 1974). The linear and nonlinear terms are separately treated at each time step. For the nonlinear part we integrate the equation

$$\frac{\partial A}{\partial\eta} = -Q(A), \tag{3.9}$$

where

$$Q(A) = \mathrm{i}\,|A|^2 A + 8\epsilon\gamma\,|A|^2\frac{\partial A}{\partial\xi} + 4\mathrm{i}\epsilon\gamma A\left.\frac{\partial\phi}{\partial\xi}\right|_{z=0}. \tag{3.10}$$

A midpoint finite-difference approximation is used for solving A. The nonlinear terms are evaluated as

$$Q[A(\xi,\eta)] = \mathrm{i}\,|A|^2 A + 8\mathrm{i}\epsilon\gamma\,|A|^2\,\mathrm{F}^{-1}\{-\nu\mathrm{F}\{A\}\} + 4\mathrm{i}\epsilon\gamma A\left.\frac{\partial\phi}{\partial\xi}\right|_{z=0}. \tag{3.11}$$

After calculating $\bar{A}(\xi, \eta+\frac{1}{2}\Delta\eta)$ by a forward difference,

$$\bar{A}(\xi, \eta+\tfrac{1}{2}\Delta\eta) = A(\xi,\eta) - \tfrac{1}{2}\Delta\eta\,Q(A(\xi,\eta)), \tag{3.12}$$

we define a new $\tilde{\bar{A}}(\xi, \eta+\Delta\eta)$ as the solution to (3.9) by

$$\tilde{\bar{A}}(\xi, \eta+\Delta\eta) = A(\xi,\eta) - \Delta\eta\,Q[\bar{A}(\xi, \eta+\tfrac{1}{2}\Delta\eta)]. \tag{3.13}$$

The linear part involves the equation

$$\frac{\partial A}{\partial\eta} + \mathrm{i}\gamma^2\frac{\partial^2 A}{\partial\xi^2} = 0. \tag{3.14}$$

The exact solution of its Fourier transform is

$$\hat{A}(\nu,\eta) = \hat{A}(\nu, 0)\exp(\mathrm{i}\gamma^2\nu^2\eta). \tag{3.15}$$

Numerically, $A(\xi, \eta+\Delta\eta)$ is obtained from $\tilde{\bar{A}}(\xi, \eta+\Delta\eta)$ by

$$A(\xi, \eta+\Delta\eta) = \mathrm{F}^{-1}\{\mathrm{F}\{\tilde{\bar{A}}(\xi, \eta+\Delta\eta)\}\exp(\mathrm{i}\gamma^2\nu^2\Delta\eta)\}. \tag{3.16}$$

To prevent minor numerical noise, the exponential factor in (3.16) is changed to $1/(1-\mathrm{i}\gamma^2\epsilon^2\Delta\eta)$ for the highest Fourier modes $\nu = \pm(N-1), \pm N$. This does not modify the solution as a whole, as these highest modes do not contribute to the wave envelope A. The solution $A(\xi,\eta)$ is thus advanced in η, and this information is then used to compute ϕ for the next step in η.

After A and ϕ are found at $2N$ grid points, A' is calculated from (2.13). To obtain ζ in (2.12) we first calculate the terms involving A between grid points by linear interpolation, and then multiply the harmonic factors involving the phase ψ.

Finally the numerical program was checked in three ways.

(i) The conservation law

$$\int_0^{2\pi} |A|^2 \, d\xi = \text{constant} \tag{3.17}$$

was verified to within 0.15 %.

(ii) The same program was applied to the CSE by taking $\epsilon = 0$ in (2.6). A soliton envelope was found to remain constant in profile up to $\eta = 50$ with an error of 10^{-3}.

(iii) The initial growth rate of the computed unstable sideband was compared with Dysthe's linearized theory. The agreement was good if $ka_0 < 0.05$.

Some remarks on the numerical efficiency are worthwhile here. In the pseudo-spectral method the nonlinear terms are evaluated at each ξ and η, through FFT, before integration in η is performed. The evaluation requires eight FFTs (cf. (3.11) and (3.13)). In addition, two FFTs are needed in the linear equation (3.14). If $2N$ Fourier modes are used, a total $O(20N \ln (2N))$ operations are needed for advancing the solution by one step in η. On the other hand, the Fourier coefficients of the Zakharov integral equation are governed by a set of coupled first-order cubic ordinary differential equations whose coefficients are double sums of $2N$ modes. For an explicit time-differencing scheme, roughly $O(2N)^3$ operations are needed per time step. Thus if the same kind of time-stepping is employed, it is much less expensive to solve Dysthe's equations for the long-time evolution of slowly varying wavetrains.

We now discuss the results of three numerical studies: periodic groups, short-wave packets and instability of a uniform wavetrain. Computational information such as grid size, etc., is given in the Appendix.

4. Periodic group

For infinitesimal waves the superposition of two progressive waves with slightly different frequencies gives rise to periodic groups whose envelopes move forward at the group velocity without change of form. Keller (1982) has recently reported experiments for such groups with maximum initial ka_0 up to 0.23. He found that each group tended to lean forward. In the spectral diagram the lower-frequency component wave (called the lower parent by Keller) remained relatively constant during the course of propagation, while the upper-frequency component (upper parent) declined. Sidebands also developed. Records at 10 stations within the first 7.14 m from the wavemaker are available.

We used Keller's initial data as inputs to our numerical scheme in the following way. From the two frequencies: $\omega_1/2\pi = 1.406$ Hz and $\omega_2/2\pi = 1.563$ Hz we defined their average $\omega/2\pi = 1.485$ Hz as the carrier-wave frequency; the corresponding k is 8.865 m^{-1}. The initial amplitude of the carrier wave was zero, while those of the parents were $\frac{1}{2}a_0 = 0.013$ m, so that $ka_0 = 0.23$. We regarded the latter as two sidebands with $\nu = \pm 1$. From the frequency difference we let $\gamma ka_0 = \Delta\omega/\omega$, so that there were two groups within the computational domain $[0, 2\pi]$. The initial condition was

$$A(x, 0) = 0.483 \, e^{i\xi} + 0.537 \, e^{-i\xi}, \tag{4.1}$$

so that the two sidebands ($\nu = \pm 1$) of $A'(x, 0)$ had equal initial amplitude of 0.5 as in the experiment. The initial values of the higher harmonic of the sidebands, i.e. $\nu = \pm 3, \pm 5$, were small in the experiments and neglected in the input. Because the nonlinear terms in (2.6) are cubic, only odd harmonics arose at later η. As shown in figure 1, the displacements ζ compare favourably with the experiments. Also the

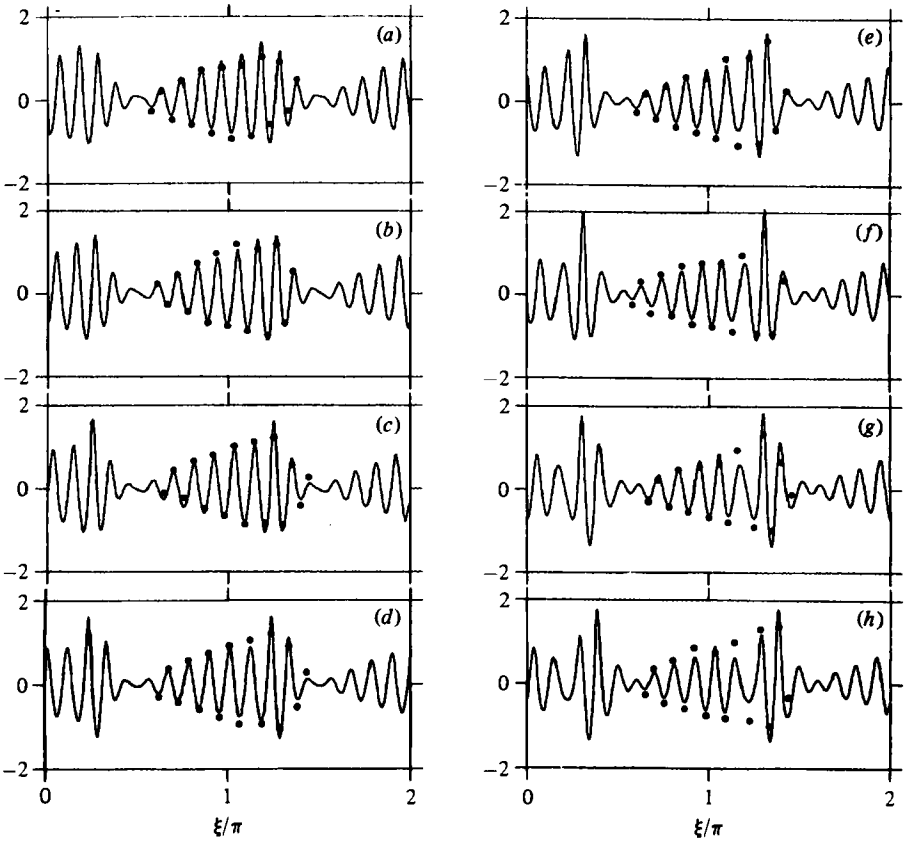

FIGURE 1. Measured and computed displacements at the last 8 stations for periodically modulated waves of Keller's experiment. ——, computed; ●, crests or troughs measured by Keller. +1 unit in the abscissa ξ/π corresponds to dimensional $\Delta t = -1/\gamma\omega k a_0$. Here $\gamma = 0.229$, $ka_0 = 0.23$, $\omega/2\pi = 1.485$ Hz and $k = 8.865$ m^{-1}. The positions x_0 of the probes are (*a*) 3.14 m, (*b*) 3.71 m, (*c*) 4.28 m, (*d*) 4.86 m, (*e*) 5.43 m, (*f*) 6.00 m, (*g*) 6.57 m, (*h*) 7.14 m. The corresponding dimensionless distance in the moving coordinates is $\eta = k^3 a_0^2 x_0$.

spectral development of the parents and their higher harmonics agrees with the observations (see figure 2). For contrast, results from the CSE are also plotted in figure 2 and are clearly unsatisfactory.

In figure 3 the spectral evolution of the envelope A' is shown for a duration much longer than that of the experiment. We further show the profiles of ζ at selected fetches in figure 4. Note that, after the envelope within the original group period splits into two groups, the higher group advances faster. Therefore the higher group from the period behind catches up and coalesces with the lower group. Recall from figure 1 (*h*) that group splitting has just begun at $\eta = 3.35$ ($x_0 = 7.14$ m). At $\eta = 5$ the splitting is complete (figure 4); the upper parent $\nu = -1$ and the lower sideband $\nu = 3$ are the greatest, while the lower parent $\nu = 1$ and the upper sideband $\nu = -3$ the smallest (figure 3). Now we can see the reason for the different group velocities most clearly. Let us interpret the larger group as the superposition of the most prominent two modes, i.e. the upper parent and lower sideband. Their average frequency is lower than the average of the upper and lower parents, i.e. ω; hence the group velocity is greater. The smaller group may be interpreted as the superposition of the lower parent and the upper sideband. Their average frequency is higher than ω; hence the group

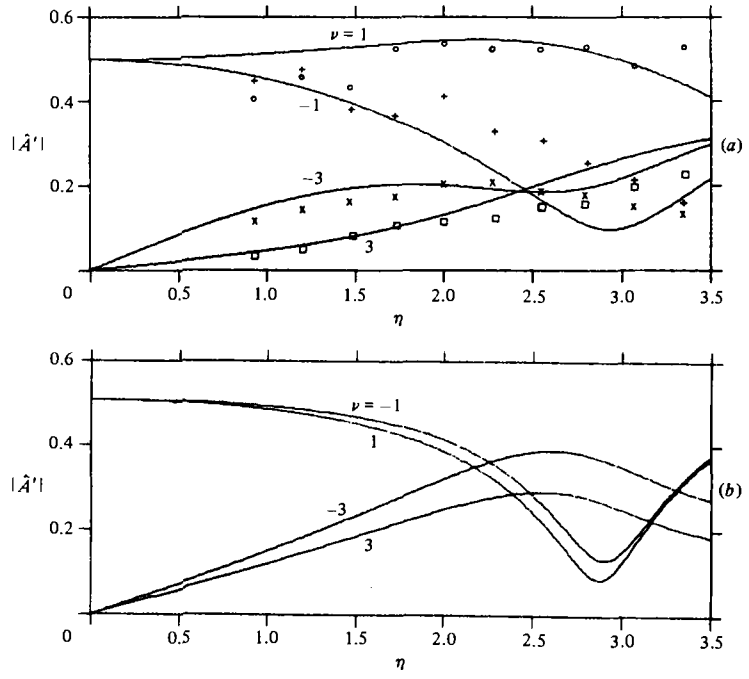

FIGURE 2. Measured and computed spectral amplitudes for periodically modulated waves. Abscissa is the dimensionless η in the moving coordinates. The probe position x_0 is related to η by $\eta = k^3 a_0^2 x_0$ with the same parameters as in figure 1. (*a*) ——, computed by present theory. Experimental measurements: +, upper parent ($\nu = -1$); ○, lower parent ($\nu = 1$); ×, upper sideband ($\nu = -3$); □, lower sideband ($\nu = 3$). (*b*) Using results by CSE.

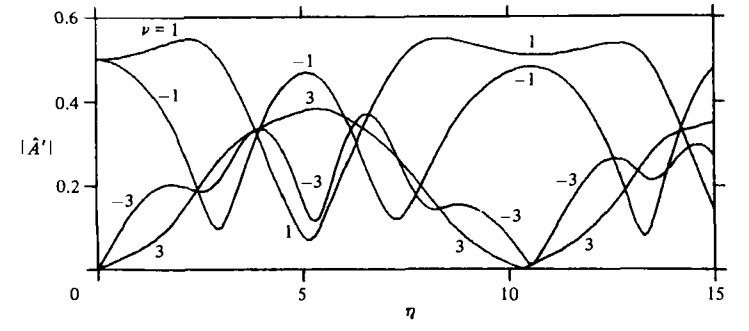

FIGURE 3. Computed long-time evolution of spectral amplitudes with the same normalizations as in figure 2.

velocity is lower. At $\eta = 8$ at the larger group from behind can no longer be distinguished from the smaller one, resulting in a single backward-leaning envelope. Continuing the overtaking, the peaks of the larger and the smaller groups coincide at $\eta = 11$; the resultant envelope is now almost symmetric as the original envelope. The upper and lower parents return to their dominance; this completes the first recurrence cycle. Thus the entire evolution process including frequency downshift is due to the unequal development of sidebands.

Finally we point out that the maximum local ka reaches as high as 0.4 at $\eta = 6$, which suggests that local breaking is likely. Keller indeed observed some breaking

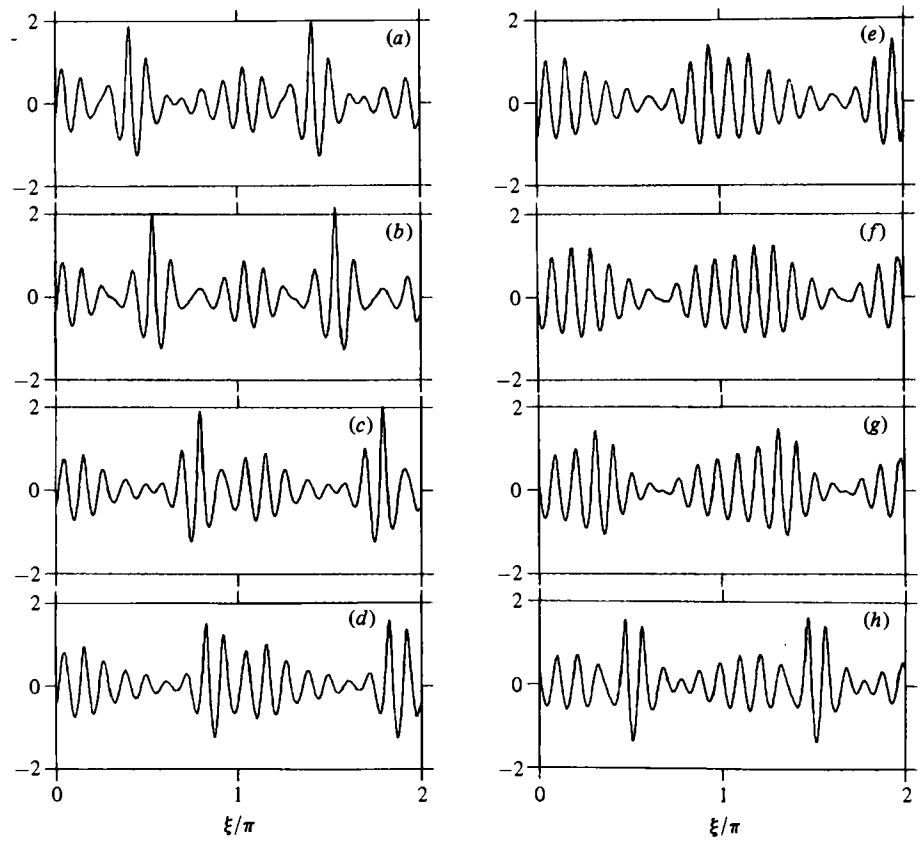

FIGURE 4. Sample computed displacements (continuation of figure 1). The dimensionless distance $\eta = k^3a_0^2x$ is (*a*) 4, (*b*) 5, (*c*) 7, (*d*) 8, (*e*) 9, (*f*) 11, (*g*) 12, (*h*) 14, with the same normalizations as in figure 1.

at the last probe corresponding to $\eta = 3.35$, where the maximum computed $ka = 0.36$. Therefore we expect their computed recurrence to be quantitatively reliable only for lower initial ka_0.

5. Short-wave packets

Feir (1967) performed experiments for packets of bell-shaped envelope and of roughly equal duration but different maximum amplitudes. Records were taken at two stations at 4 and 28 feet from the wavemaker. For low wave slope the envelopes remained symmetrical and flattened with distance. For relatively steep waves, however, the envelopes first steepened forward, then split into two groups with the smaller group trailing. Using 15 modes in the mode-coupling equations of West *et al.* (1974), Cohen *et al.* (1976) simulated numerically the experiments of Feir (1967). The computation was carried out only to a time when asymmetry and group splitting were beginning to show. More extensive experiments in a long tank for initially square envelopes with $ka_0 = 0.09$–0.28 have been reported by Su (1982).† Free-surface displacements are available at eight stations from 6.1 m to 106.7 m from the wave-

† Similar data were also reported by Chereskin (1982), whose experiments were performed in Su's tank.

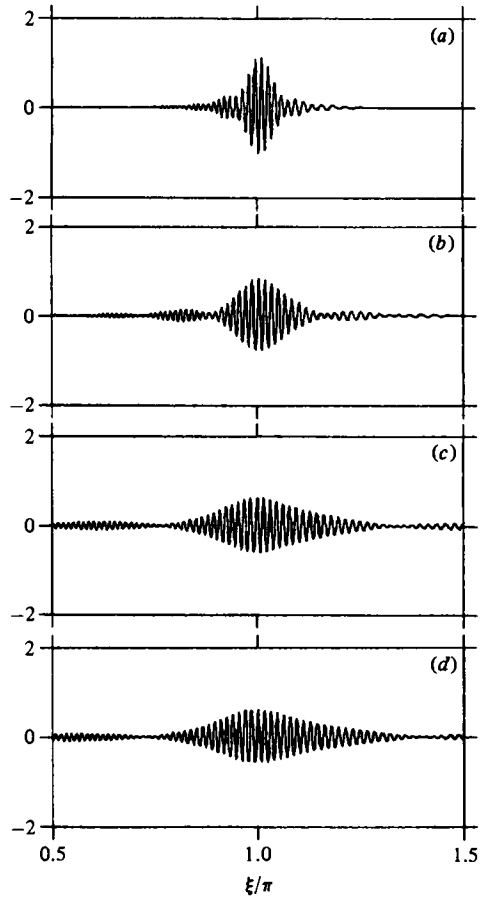

FIGURE 5. Computed free surface of short wave packet at sample probes of Su's experiment. The probe positions x_0 are (*a*) 18.3 m, (*b*) 42.7 m, (*c*) 91.5 m, (*d*) 106.7 m. Initial $ka_0 = 0.09$, $\omega/2\pi = 0.96$ Hz and $\omega T = 10\pi$. +1 unit in the abscissa ξ/π corresponds to dimensional $\Delta t = -1/\gamma\omega k a_0$; $\gamma = 0.0868$.

maker. They confirmed Feir on the asymmetry of evolution and further revealed that the separated groups have different frequencies.

In this section we report our simulation of three experimental cases studied by Su for further insight: $ka_0 = 0.09$ with 5 and 10 waves in the original envelope, and $ka_0 = 0.15$ with 10 waves. Longer packets with 20 and 60 waves were also tested by Su, but would require substantially greater computational effort and are not pursued here. The initial condition was taken to be

$$A(\xi, 0) = 0.5[\tanh(j - j_a) - \tanh(j - j_b)], \quad j = 1, 2, \ldots, 2N,$$

where $(j_b - j_a)\Delta x$ was the initial length of the packet. As defined, the ends were slightly smoothed to avoid numerical instability. For the computational domain of $\xi \in [0, 2\pi]$ the dimensional range of time t is $2\pi/\gamma\omega ka$. We always chose γ so that this time range was much longer than the total duration of the evolving packets.

Figure 5 shows the computed free surface ζ for the shortest packet with $ka_0 = 0.09$ and $\omega/2\pi = 0.96$ Hz. The initial duration of the packet is $\omega T = 10\pi$. The results are very close to the measurements. This is a case where the initial packet is too small to emit a soliton according to the CSE. Note in particular the slightly asymmetric

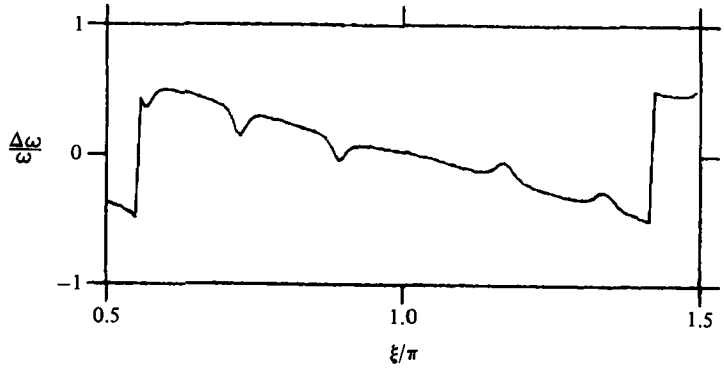

FIGURE 6. Frequency deviation $\Delta\omega/\omega$ at $x_0 = 42.7$ m for the same parameters as in figure 5.

	$ka_0 = 0.09$				$k_0 a_0 = 0.15$,	
	$\omega T = 10\pi$		$\omega T = 20\pi$		$\omega T = 20\pi$	
x_0 (m)	Measured	Computed	Measured	Computed	Measured	Computed
6.1	0.107	0.106	0.115	0.099	0.218	0.175
18.3	0.120	0.093	0.127	0.101	0.232	0.228
24.4	0.094	0.089	0.129	0.118	0.289	0.295
42.7	0.073	0.072	0.166	0.138	0.232	0.249
61.0	0.066	0.063	0.147	0.140	0.142	0.225
76.3	0.053	0.059	0.135	0.142	0.125	0.267
91.5	0.049	0.058	0.132	0.139	0.130	0.239
106.7	0.047	0.052	0.131	0.138	0.138	0.253

TABLE 1. Measured and computed maximum local ka_0 at the probes of Su's experiments

envelope between $x_0 = 42.7$ m and $x_0 = 91.5$ m, which is also noticeable in Su's records. The wave period is also longer in the low group in front of the main group. In particular the backward-leaning of the main group is associated with the nonlinear modification of linear dispersion. Figure 6 shows a sample distribution of frequency deviation $\Delta\omega$ from ω at $x_0 = 42.7$ m. Note that there is a general tendency of frequency downshift ($\Delta\omega < 0$) in front of the main peak, and upshift $\Delta\omega > 0$ behind. Therefore the front of the main envelope is steepened. The local extrema in $\Delta\omega$ correspond to the nodes of ζ, where the phase is meaningless. Quantitatively we have compared the measurement and the theory for the maximum amplitude at the peak of the largest group, at all 8 stations, as listed in table 1. The agreement is fairly good, despite the fact that no dissipation is accounted for in our theory. Because of the small scale of Su's plots, more detailed comparison is difficult and is not made here.

Figure 7 gives the theoretical free surface for a packet having twice the duration ($\omega T = 20\pi$) but identical values of ka_0 and carrier frequency as in the preceding case. The results showing the development of groups are again quantitatively close to Su's measurements for all eight stations; the maximum amplitudes are compared in table 1 also. Note here that the frequency downshift is very evident in the leading group. The corresponding 3-dimensional view of the computed first harmonic envelope A' is shown in figure 8. The very low leading group advances faster than C_g, and than

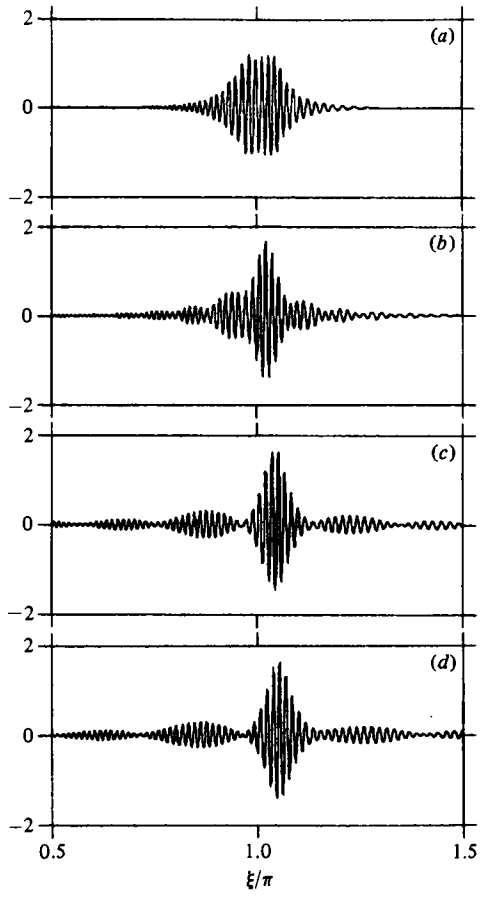

FIGURE 7. As figure 5 except $\omega T = 20\pi$.

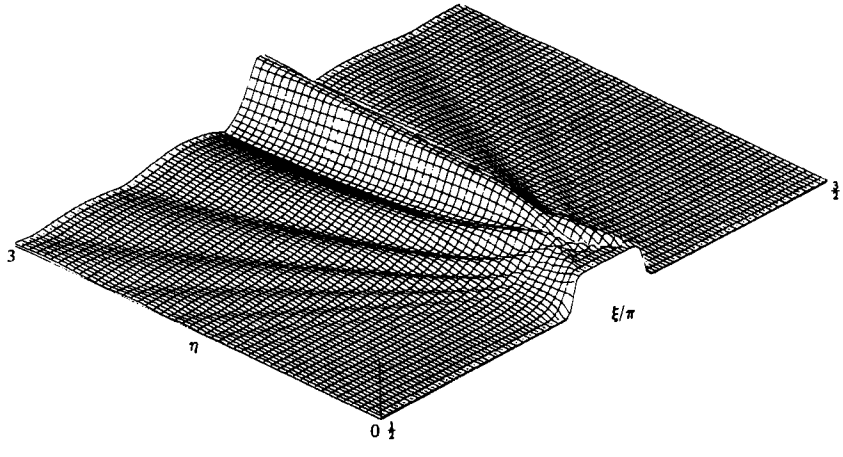

FIGURE 8. Overall evolution of A' in moving coordinates. Initial $ka_0 = 0.09$, $\omega/2\pi = 0.96$ Hz, $\omega T = 20\pi$ and $\gamma = 0.0868$.

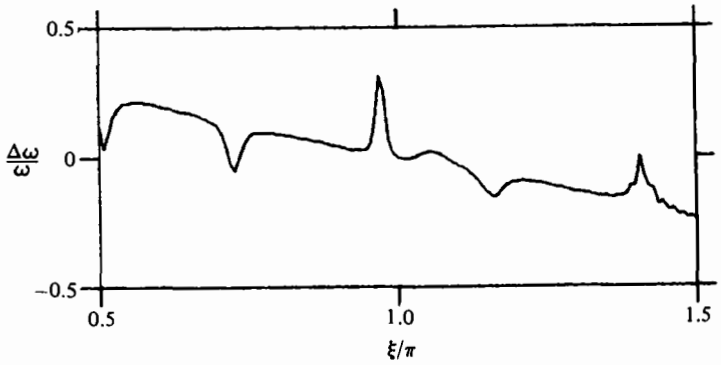

FIGURE 9. Frequency deviation $\Delta\omega/\omega$ at $x_0 = 106.7$ m for the same parameters as in figure 7.

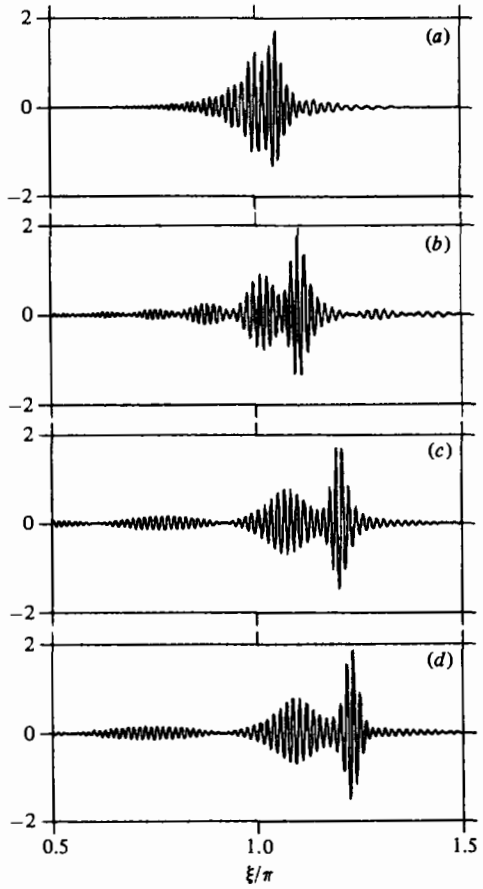

FIGURE 10. As figure 5 except initial $ka_0 = 0.15$, $\omega/2\pi = 1.12$, $\omega T = 20\pi$ and $\gamma = 0.0521$.

all other groups. We also display in figure 9 the frequency deviation $\Delta\omega$ at $x_0 = 106.7$ m. There is downshift in the leading group ahead of the main and highest group, no significant frequency change in the main group, but upshift in the groups behind.

Figure 10 is for the steeper waves $ka_0 = 0.15$, $\omega/2\pi = 1.12$ Hz and $\omega T = 20\pi$. Agreement with Su's experiment is good up to $x_0 = 42.7$ m. Since in the measure-

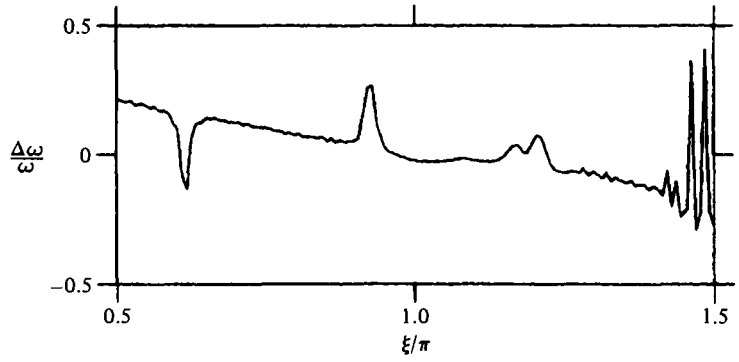

FIGURE 11. Frequency deviation $\Delta\omega/\omega$ at $x_0 = 91.5$ m for the same parameters as in figure 10.

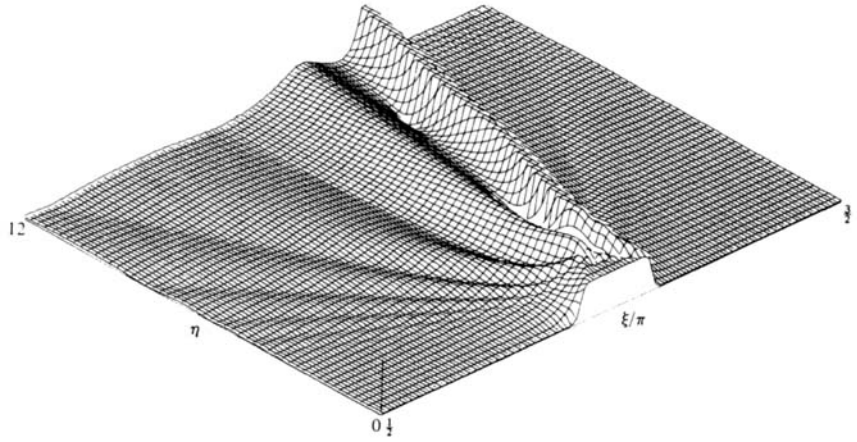

FIGURE 12. Overall evolution of A' in moving coordinates. Initial $ka_0 = 0.15$, $\omega/2\pi = 1.12$, $\omega T = 20\pi$ and $\gamma = 0.0521$.

ments there is a sudden drop of amplitude from $x_0 = 42.7$ to 61.0 m, signifying the occurrence of breaking, the quantitative discrepancy after $x_0 = 61$ m is understandable. In spite of this, frequency downshift can be seen now in the largest group just as in the observations. This is further displayed by the frequency deviation for $x_0 = 91.5$ m in figure 11. Figure 12 gives the overall evolution of A'. The leading and highest group advances faster than the longest group, which in turn travels faster than the group velocity of the original carrier waves; this is consistent with the frequency downshift in the leading group. *Thus the groups must eventually separate totally from one another.* This feature has not been convincingly established before.

We recall from the exact solution of CSE by Zakharov & Shabat (1972) that an envelope pulse, whatever its initial shape, evolves into a finite number of envelope solitons plus minor oscillations that decay with time, if the total area of the initial pulse is sufficiently large. The decaying oscillations are the consequence of linear dispersion and can be inferred from the linear part of CSE. If $A(\xi, 0)$ is real the solitons are stationary in (ξ, η)-coordinates. The interaction among these *bound* solitons is exhibited by the presence of envelope nodes which recur at definite periods. Hence there is no total separation of groups, *in contrast* with the present computations on the basis of a more accurate theory and with Su's experiments.

Since dissipation affects the results only in a quantitative way we may now

conclude that a short wave packet can evolve into groups which ultimately separate, because of the frequency downshift in the leading group. The separated groups resemble, but are not exactly, the usual solitons. We have studied numerically wave envelopes which are initially single stable solitons according to the CSE. These envelopes now propagate faster if the maximum amplitudes are higher, while the peaks undergo minor undulations. Analytical soliton solutions for Dysthe's equation have not been found.

In addition to the larger cost of computation for those very long packets experimented by Su, our reason for not carrying out the numerical theory for them was that the shorter packets already gives a sufficiently clear physical picture. More groups are expected to split from a longer packet. Groups in the central part of the packet would evolve in ways similar to those in an infinitely long train of unstable waves, to be studied in §6, until end effects encroach toward the centre, which would lead to ultimate separation.

6. Sideband instability with dissipation

Numerical experiments by Yuen & Lake (1982), based on the discretized Zakharov integral equation and 7 modes (the carrier-wave mode $\nu = 0$, and the sidebands and their higher-harmonic modes ± 1, ± 2, ± 3), and by Bryant (1982), using up to 29 modes, have revealed the following.

(i) If only the sideband modes $\nu = \pm 1$ are linearly unstable, the lower mode $(+1)$ grows faster than the upper mode (-1), while the carrier wave diminishes. After a time the trends are reversed and continued by nearly recurring rises and falls. The greatest difference between modes $+1$ and -1 occurs when both attain their maxima. If the initial wave slope ka_0 is large enough, $\max(\hat{A}_1')$ can exceed $\min(\hat{A}_0')$, thereby causing temporary frequency downshift. This agrees qualitatively with the observations of Lake *et al.* (1977, figure 3) and Melville (1982, figure 4). The higher modes, which are linearly stable, follow passively the rises and falls of the modes ± 1, except that $\max \hat{A}_\nu' < \max \hat{A}_{-\nu}'$, $\nu > 2$.†

(ii) If the initial wave slope is quite large ($ka_0 > 0.2$, but below the threshold of restabilization) so that two or more pairs of sidebands are linearly unstable, then recurrence ceases to exist. The more numerous the unstable sidebands, the more chaotic the subsequent evolution. Our numerical experiments for moderately high ka_0 and without dissipation confirm the findings of Yuen & Lake and Bryant and need not be reported here.

Based on the simplified Dysthe equations, Janssen (1983) has considered the special case where the lowest sidebands are close to the threshold of instability. He finds that $\max \hat{A}_1' < \max \hat{A}_{-1}'$ instead. This inequality remains valid even when the full equations are used, as pointed out by a referee for small time and confirmed numerically by us for small and large time.

Laboratory experiments by Lake *et al.* (1977) and Melville (1982) were conducted in a relatively short tank and fairly large values of initial ka_0 were used. The unstable sidebands grew so large at the first maxima that breaking was sometimes observed. Therefore events near the first sideband maximum and afterwards cannot be checked by available theories. In order to see what could happen to two-dimensional waves of moderate steepness ($ka_0 < 0.15$, for example) in a very long tank, we have

† In the absence of viscosity the inequality $\max \hat{A}_\nu < \max \hat{A}_{-\nu}$ for all ν except $\nu = 1$ could be inferred from the second invariant in equation 18) of Janssen (1983), for the simplified Dysthe equations. The invariant does not, however, hold for the full equations.

examined the effect of dissipation, which may be important when very long time is considered. It is of course well known that, in addition to viscous dissipation, meniscus and surface aging or contamination can greatly affect the damping rate quantitatively and possibly qualitatively; but the physics of all except the first is not well understood to be given a rigorous description. Hence we shall adopt the conventional parametric model by adding a linear term δA to the left of (2.1) as was done in numerical experiments by Chu & Mei (1971) and analytically by Segur (1981). If viscosity in the wall boundary layers is the dominant source of dissipation, then, according to the linearized theory for deep water waves,

$$\delta = \left(\frac{\nu\omega}{2}\right)^{\frac{1}{2}} \frac{1}{B}(1-\mathrm{i}), \tag{6.1a}$$

where B is the tank width. In the normalized equation (2.6) we add $\hat{\delta}A$, where

$$\hat{\delta} = \left(\frac{2\nu}{\omega}\right)^{\frac{1}{2}} \frac{1-\mathrm{i}}{B(ka_0)^2}. \tag{6.1b}$$

Taking the following values typical in a laboratory tank,

$$B = 1 \text{ m}, \quad \nu = 1\times 10^{-6} \text{ m}^2/\text{s}, \quad f = 2 \text{ Hz},$$

we find

$$\hat{\delta} = \frac{4(1-\mathrm{i})\times 10^{-4}}{(ka_0)^2}, \tag{6.2}$$

which means that damping can be appreciable during the time range for which Dysthe's equations hold. Note, however, that, in the open ocean or a very wide tank, the viscous-damping factor is

$$\delta = 2\nu k^2, \tag{6.3a}$$

whose dimensionless form is

$$\hat{\delta} = \frac{4\nu k^2}{(ka_0)^2\omega}. \tag{6.3b}$$

Even if ν is taken to be 100 times the laminar viscosity, the factor is still only $10^{-6}/(ka_0)^2$ for a wave of 10 s period. Thus damping, if important in nature, is caused by other effects. Furthermore, in wide tanks or real seas nonlinear evolution may be complicated by three-dimensional instabilities (see McLean *et al.* 1981; Melville 1982).

In the results to be presented, the initial disturbance consisted of a pair of sidebands $\nu = \pm 1$ but not their higher harmonics,

$$A(\xi, 0) = 1 + S(\mathrm{e}^{\mathrm{i}\xi} + \mathrm{e}^{-\mathrm{i}\xi})\,\mathrm{e}^{\mathrm{i}\alpha}, \tag{6.4}$$

where S and α are the initial amplitude and phase respectively of the sidebands. According to Dysthe's linearized criterion, the sidebands $\nu = \pm 1$ are unstable for

$$\frac{\Delta k}{k} = 2\gamma k a_0 < 2\sqrt{(2)}\, ka_0 (1 - 2\gamma k a_0)^{\frac{1}{2}}. \tag{6.5}$$

The maximum growth rate in time is

$$\mathrm{Im}\,\Delta\omega/\omega = \tfrac{1}{2}(1-2ka_0)(ka_0)^2, \tag{6.6}$$

which occurs at $\gamma = 1 - \frac{3}{2}ka_0$. The initial phase α is $-\frac{1}{4}\pi$ for maximum linear growth at small time (Benjamin & Feir 1967; Stiassnie & Kroszynski 1982). In our

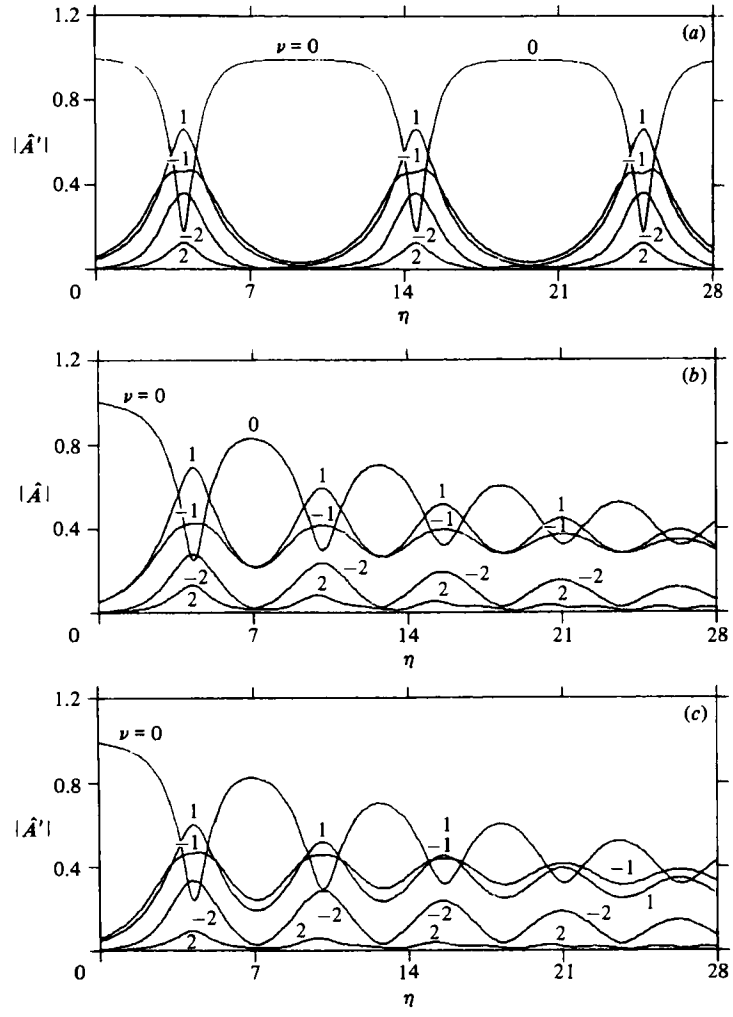

FIGURE 13. Variation of spectral amplitudes $\nu = 0, \pm 1, \pm 2$ for modulated wave-train versus dimensionless η in moving coordinate. $ka_0 = 0.15$ and $\gamma = 0.775$; (*a*) inviscid result for A'; (*b*) with dissipation for A; (*c*) with dissipation for A'.

computations the initial amplitude S is fixed at 0.05. Owing to dissipation, the conservation law (3.17) is modified to

$$\left(\int |A|^2 \, d\xi\right)_\eta = \left(\int |A|^2 \, d\xi\right)_{\eta=0} e^{-2\hat{\delta}\eta}. \tag{6.7}$$

This relation is satisfied to a high degree of accuracy in all our computations.

First we consider only one pair of sidebands, which are the most unstable ($\gamma = 0.755$) according to (6.5). All high harmonics are linearly stable. The carrier wave has the initial $ka_0 = 0.15$. For comparison, the inviscid results are presented in figure 13 (*a*). The Fourier components of $A'(\xi, \eta)$ which include the carrier wave ($\nu = 0$) and its sidebands ($\nu = \pm 1, \pm 2$) are plotted against the normalized distance η. With dissipation the Fourier components of A are shown in figure 13 (*b*), where $\hat{\delta}$ is given by (6.2), and the Fourier components of A' in figure 13 (*c*). As in the inviscid case, the upper ($\nu = -1$) and lower ($\nu = +1$) sidebands grow and decay in a quasi-recurring

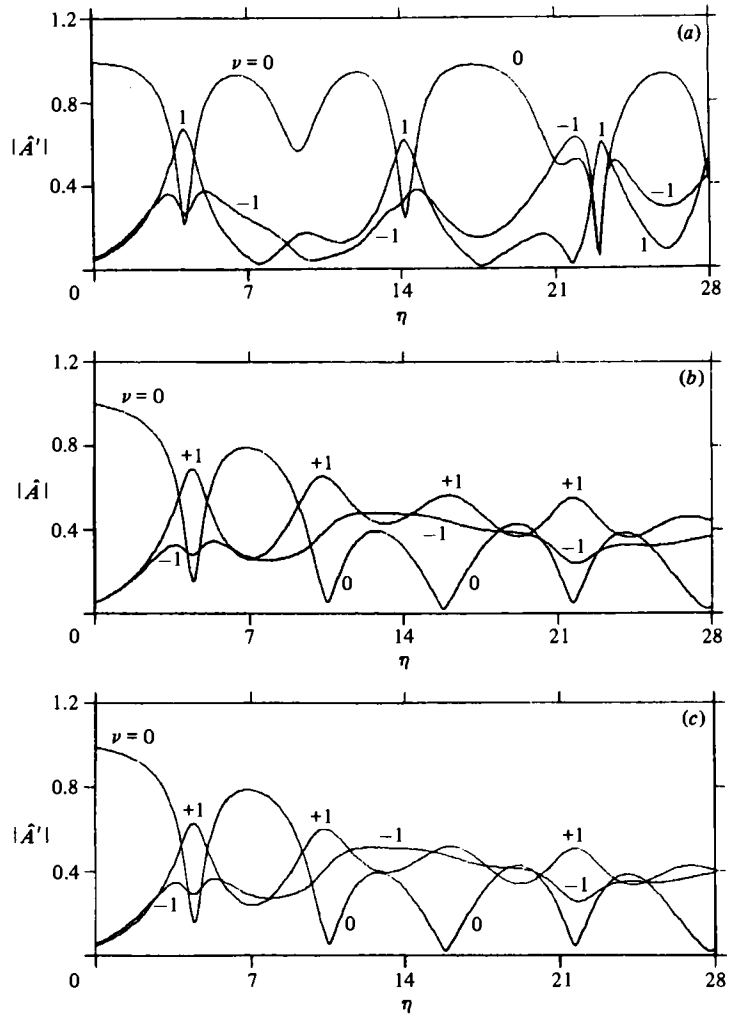

FIGURE 14. As figure 13 except $\gamma = 0.5$ and $\nu = 0, \pm 1$.

manner, with the lower sideband dominant at the first maxima. However, with dissipation, the cyclic pattern is shortened and recurrence is accompanied by attenuation. The maxima of the lower sideband of A continue to be greater than those of the upper sideband; this is not so for A' because the term $\partial A/\partial\xi$ in (2.13) accentuates the upper sideband.

The cases where two pairs of sidebands $\nu = \pm 1, \pm 2$ are linearly unstable according to (6.5) are presented in figures 14 and 15, where $ka_0 = 0.15$ and initial data (6.4). Here we take $\gamma = 0.5$. For comparison, the inviscid results for A' are plotted in figures 14(*a*) and 15(*a*); recurrence is obscured. With damping, the upper sideband of A, $\nu = -1$, grows from its initial small value and then remains fairly flat throughout, figure 14(*b*). The lower sideband of A, $\nu = 1$, rises and falls with attenuation, alternates with the carrier, $\nu = 0$, and dominates over the upper sideband most of the time. The higher unstable sideband pair, $\nu = \pm 2$, remains fairly passive throughout. As for the Fourier components of A' (figure 14*c*), the lower sideband, $\nu = 1$, is comparable to the upper sidebands, $\nu = -1$. Computations by doubling the

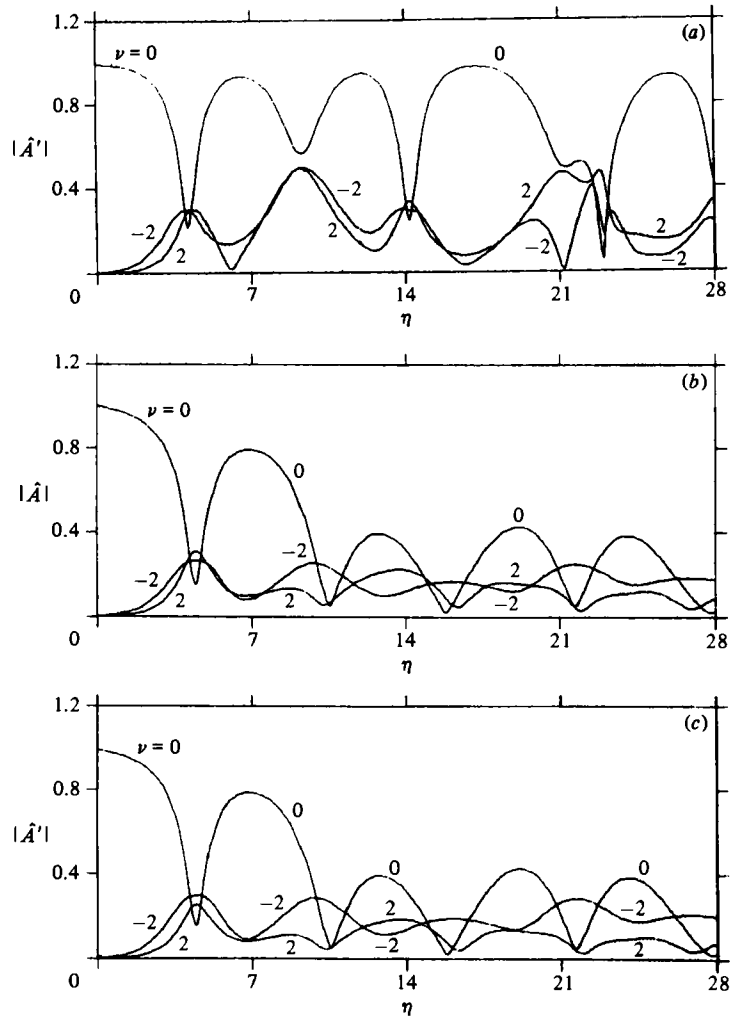

FIGURE 15. As figure 13 except $\gamma = 0.5$ and $\nu = 0, \pm 2$.

damping give similar results. We have further examined† the same initial state but with twice the total number of Fourier modes so that four sideband pairs are now unstable. The new modes have one-half and three-halves of the wavenumber of the pair that was assigned a non-zero initial value. These new modes can grow from minute numerical noise (with an assigned initial value of 10^{-6} in our tests) and lead to a more chaotic state after a long time, *if viscosity is ignored*. However, with viscosity as modelled here, their unstable growth is virtually completely suppressed.

New experiments for mild wave slopes ($ka_0 < 0.15$) over a long fetch (beyond the first maximum of the sidebands) are needed to check these computed results.

7. Concluding remarks

From the reasonable agreement between recent experiments and our computations, both for initially periodic groups and for wave packets, it appears that Dysthe's extension of the CSE is a useful basis for predicting the long-time evolution of

† At the suggestion of a referee.

narrow-banded weakly nonlinear waves. From §6, viscous effects in a typical laboratory tank are seen to be significant within the time range $(ka)^3\omega t = O(1)$ to which Dysthe's extension is limited. Because of this, viscosity would be dominant in a longer time range $(ka)^3\omega t \gg 1$, and further extension of Dysthe's equations does not seem worthwhile, if ka and the bandwidth are sufficiently small. For either broad bandwidth or large ka, modulation is no longer slow. In the former case one can use Zakharov's integral equation, while, in the latter, the exact numerical theory is needed.

This research has been jointly sponsored by the Fluid Mechanics Programs of the U.S. National Science Foundation and the Office of Naval Research. We acknowledge fruitful discussions on the experimental aspects of this topic with Professor W. K. Melville and Dr N. Huang, and on numerical techniques with Professor S. A. Orszag. Special thanks are due to G. Keller whose unpublished experimental data prompted §4.

REFERENCES

Benjamin, T. B. & Feir, J. E. 1967 The disintegration of wave trains in deep water. Part 1. Theory. *J. Fluid Mech.* **27**, 417–430.

Bryant, P. J. 1982 Modulation by swell of waves and wave groups on the ocean. *J. Fluid Mech.* **114**, 443–446.

Chereskin, T. K. 1982 The development of nonlinear surface and internal wave groups. Doctoral thesis, Woods Hole/MIT Joint Program in Oceanography and Ocean Engineering.

Chu, V. H. & Mei, C. C. 1970 On slowly varying Stokes waves. *J. Fluid Mech.* **41**, 873–887.

Chu, V. H. & Mei, C. C. 1971 The nonlinear evolution of Stokes waves in deep water. *J. Fluid Mech.* **47**, 337–351.

Cohen, B. I., Watson, K. M. & West, B. J. 1976 Some properties of deep water solitons. *Phys. Fluids* **19**, 345–354.

Crawford, D. R., Lake, B. M., Saffman, P. G. & Yuen, H. C. 1981 Stability of weakly nonlinear deep water waves in two and three dimensions. *J. Fluid Mech.* **105**, 177–191.

Dysthe, K. B. 1979 Note on a modification to the nonlinear Schrödinger equation for application to deep water waves. *Proc. R. Soc. Lond.* A **369**, 105–114.

Feir, J. E. 1967 Discussion: some results from wave pulse experiments. *Proc. R. Soc. Lond.* A **299**, 54–58.

Fornberg, B. & Whitham, G. B. 1978 A numerical and theoretical study of certain nonlinear wave phenomena. *Phil. Trans. R. Soc. Lond.* A **289**, 373–404.

Janssen, P. A. E. 1983 On a fourth-order envelope equation for deep-water waves. *J. Fluid Mech.* **126**, 1–11.

Keller, G. J. 1982 Experiments on nonlinear wave interaction (private communication).

Lake, B. M., Yuen, H. C., Rungaldier, H. & Ferguson, W. E. 1977 Nonlinear deep water waves: theory and experiment. 2. Evolution of a continuous wave train. *J. Fluid Mech.* **83**, 49–74.

Longuet-Higgins, M. S. 1978 The instabilities of gravity waves of finite amplitude in deep water. II. Subharmonics. *Proc. R. Soc. Lond.* A **360**, 489–505.

McLean, J. W., Ma, Y. C., Martin, D. U., Saffman, P. G. & Yuen, H. C. 1981 A new type of three dimensional instability of finite amplitude gravity waves. *Phys. Rev. Lett.* **46**, 817–820.

Melville, W. K. 1982 The instability and breaking of deep-water waves. *J. Fluid Mech.* **115**, 165–185.

Roskes, G. J. 1977 Fourth order envelope equation for nonlinear dispersive gravity waves. *Phys. Fluids* **20**, 1576–1577.

Segur, H. 1981 Viscous decay of envelope solitons in water waves. *Phys. Fluids* **24**, 2372–2374.

Stiassnie, M. 1984 Note on the modified Schrödinger equation for deep water waves. *Wave Motion* **6**, 431–433.

STIASSNIE, M. & KROSZYNSKI, U. I. 1982 Long-time evolution of an unstable water-wave train. *J. Fluid Mech.* **116**, 207–225.

SU, M. Y. 1982 Evolution of groups of gravity waves with moderate to high steepness. *Phys. Fluids* **25**, 2167–2174.

TAPPERT, F. 1974 Numerical solutions of the Korteweg–de Vries equation and its generalizations by the split-step Fourier method. *Lectures Appl. Maths* **15**, 215–216.

WEST, B. J., WATSON, K. M. & THOMSON, A. J. 1974 Mode coupling description of ocean wave dynamics. *Phys. Fluids* **17**, 1059–1067.

YUEN, H. C. & FERGUSON, W. E. 1978 Relationship between Benjamin–Feir instability and recurrence in the nonlinear Schrödinger equation. *Phys. Fluids* **21**, 1275–1277.

YUEN, H. C. & LAKE, B. M. 1982 Nonlinear dynamics of deep water gravity waves. *Adv. Appl. Mech.* **22**, 67–229.

ZAKHAROV, V. E. & SHABAT, A. B. 1972 Exact theory of two-dimensional shelf-focusing and one-dimensional self-modulation of waves in nonlinear media. *Sov. Phys. JETP* **34**, 62–69.

Appendix. Computational data

Case	Number of mesh points in $x \in [0, 2\pi]$ $2N$	Time step Δt	γ	$k_0 a$	Comments ωT	j_a	j_b
Periodic group	64	0.0025	0.229	0.23			
Short packets	256	0.01	0.0868	0.09	10π	124	134
	256	0.01	0.0868	0.09	20π	119	139
	256	0.01	0.0521	0.15	20π	119	139
Wavetrain instability with and without dissipation	64	0.0025	0.775	0.15			
	64	0.0025	0.5	0.15			